JACS
JOURNAL OF THE AMERICAN CHEMICAL SOCIETY
Article
pubs.acs.org/JACS

Six-Color Time-Resolved Förster Resonance Energy Transfer for Ultrasensitive Multiplexed Biosensing

Daniel Geißler,[†] Stefan Stufler,[‡] Hans-Gerd Löhmannsröben,[†] and Niko Hildebrandt*[,§]

[†] Physical Chemistry, University of Potsdam, 14476 Potsdam-Golm, Germany
[‡] NanoPolyPhotonics, Fraunhofer Institute for Applied Polymer Research, 14476 Potsdam-Golm, Germany
[§] Institut d'Electronique Fondamentale, Université Paris-Sud, 91405 Orsay Cedex, France

Supporting Information

ABSTRACT: Simultaneous monitoring of multiple molecular interactions and multiplexed detection of several diagnostic biomarkers at very low concentrations have become important issues in advanced biological and chemical sensing. Here we present an optically multiplexed six-color Förster resonance energy transfer (FRET) biosensor for simultaneous monitoring of five different individual binding events. We combined simultaneous FRET from one Tb complex to five different organic dyes measured in a filter-based time-resolved detection format with a sophisticated spectral crosstalk correction, which results in very efficient background suppression. The advantages and robustness of the multiplexed FRET sensor were exemplified by analyzing a 15-component lung cancer immunoassay involving 10 different antibodies and five different tumor markers in a single 50 μL human serum sample. The multiplexed biosensor offers clinically relevant detection limits in the low picomolar (ng/mL) concentration range for all five markers, thus providing an effective early screening tool for lung cancer with the possibility of distinguishing small-cell from non-small-cell lung carcinoma. This novel technology will open new doors for multiple biomarker diagnostics as well as multiplexed real-time imaging and spectroscopy.

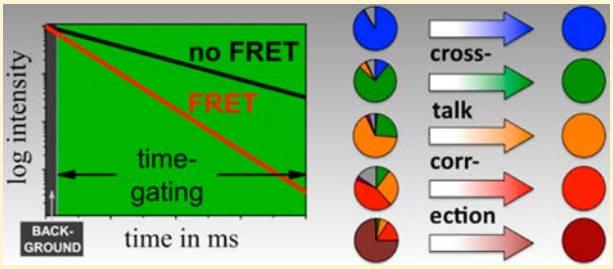

INTRODUCTION

The growing interest in complicated biomolecular systems, in which several different interacting molecules are responsible for the overall function of the system (e.g., in live cell investigations), and the increasing demand for multiparameter chemical and biological sensing (e.g., in clinical diagnostics) have made simultaneous monitoring of different binding events at extremely low concentrations an important requirement for many biosensing applications.[1−5] Förster resonance energy transfer (FRET) is a distance-dependent energy transfer between an excited donor and a non-excited acceptor separated by a distance of ca. 1−20 nm.[6−9] As many biomolecular interactions occur in this distance range, FRET is frequently used for the analysis of biomolecular structures and dynamics ranging from single binding pairs to simultaneous monitoring of multiple processes.[10−18] Apart from sensing, multicolor FRET has also been successfully exploited for the creation of signals, e.g., in DNA machines and optical switches toward DNA computing.[19−22] The parallel detection of several molecular interactions can only be realized by multiparametric approaches, such as optical multiplexing, with many different fluorophores emitting from the UV to the NIR spectral region being commercially available.[22,23] Semiconductor quantum dots offer several spectroscopic advantages over organic dyes,[24] and proofs-of-concept for ultrasensitive multiplexed biosensing have already been demonstrated.[25] However, their large sizes and difficulties in stable and functional bioconjugation have so far hampered their application in commercial diagnostics.[26] Conjugation of organic dyes to many different biomolecules can be easily performed without significantly altering the biological functions of the fluorescent bioconjugates,[27,28] but for multiplexed approaches the spectral overlap problems (cf. Figure 1) need to be overcome in order to realize limits of detection (LODs) in the sub-nanomolar or even sub-picomolar concentration range. This is absolutely necessary in order to transfer proof-of-concept studies (which often achieve only micromolar or nanomolar LODs) into useful and widely applicable biological and chemical sensors. Today, commercial bioassays with such low LODs can only be found for single analyte detection.

In order to achieve the challenging requirement of detecting extremely low concentrated samples in real-life multiplexed biosensing, we developed a combination of lanthanide-based time-gated FRET and efficient spectral crosstalk correction. Multiplexed FRET from Tb-based complexes to different dyes has already been successfully applied to immunoassays,[29,30] the monitoring of peptide−protein interactions,[31] and the investigation of ligand-regulated protein−protein exchange processes.[32] However, very low (sub-nanomolar) LODs could only be realized for single or double FRET assays, and all these studies were limited to a maximum of three acceptor dyes. Here

Received: October 18, 2012
Published: December 11, 2012

dx.doi.org/10.1021/ja310317n | J. Am. Chem. Soc. 2013, 135, 1102−1109

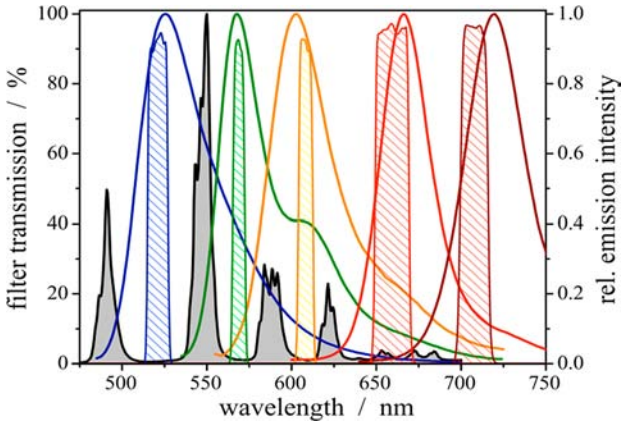

Figure 1. Luminescence spectra of the Tb donor (black curve with gray background) and acceptor dyes (colored solid lines; dye1 to dye5 from left to right) as well as transmission spectra of the used detection bandpass filters (colored lines with shaded background).

we present a significant improvement of the approaches mentioned above by demonstrating a six-color FRET (one Tb complex donor and five organic dye acceptors) experiment combined with a spectral crosstalk correction algorithm for each optical detection channel to realize ultrasensitive (low picomolar LODs) biosensing. Relatively large Förster distances (between 4.4 and 6.0 nm, cf. Supporting Table 1) for the different Tb–dye FRET pairs ensure efficient 5-fold multiplexed FRET. In contrast to our previous six-color FRET proof-of-principle studies using quantum dot acceptors (without crosstalk correction),[25] we challenged our Tb-to-dye FRET system with the selective diagnosis of small-cell and non-small-cell lung carcinoma (SCLC and NSCLC) in human serum, a highly relevant topic for early-stage screening and effective therapy monitoring, which may avoid painful and traumatizing lung biopsies.[33−36] The use of commercially available antibodies, Tb complexes, and organic dyes, as well as standard optical bandpass filters for spectral separation of the Tb donor and the different dye acceptors (which could also be replaced by fluorescent proteins or other multicolor acceptors), demonstrates the general applicability of our multiplexed FRET technology for simultaneous monitoring of multiple biological processes with time-gated optical spectroscopy and imaging.

MATERIALS AND METHODS

Donor and Acceptors. The donor fluorophore was the commercial luminescent Tb complex Lumi4-Tb (Lumiphore Inc., CA), named Tb throughout the manuscript. Detailed structural and photophysical information about this complex is given elsewhere.[37] The acceptor fluorophores were the commercial organic dyes OregonGreen 488 (dye1), AlexaFluor 555 (dye2), AlexaFluor 568 (dye3), Cy5 (dye4), and AlexaFluor 700 (dye5) (dye1, dye2, dye3, and dye5 from Invitrogen/Life Technologies; dye4 from GE Healthcare). The emission spectra of donors and acceptors are shown in Figure 1. Other photophysical properties are given in Table 1.

Tumor Marker (TM) and Antibody (AB) Samples. One of the most important aspects for lung cancer diagnostics is the distinction between rapidly growing aggressive neoplasm with high sensitivity to chemo- and radiotherapy (SCLC) and adenocarcinoma, squamous cell carcinoma, and large cell carcinoma (NSCLC) which are usually late diagnosed and poorly sensitive to chemo- and radiotherapy.[36,38] As a clear diagnosis of SCLS and/or NSCLC is not possible with a single biomarker, a combination of different TMs must be used. The different concentration levels in serum can then be related to each other for a specific and sensitive diagnosis. This approach has shown to be very successful for efficient lung cancer diagnosis.[38,39] For our multiplexed lung cancer assay we used five of the TMs proposed to allow high specificity for SCLC or NSCLC in combination with high sensitivity. These five TMs are neuron-specific enolase (NSE), carcinoembryonic antigen (CEA), the cytokeratin-19 fragment Cyfra21-1, squamous cell carcinoma antigen (SCC), and the carbohydrate antigen CA15.3.[36,38,39] Commercially available immunoassay kits for the KRYPTOR immunoreader already exist for the detection of all of these TMs (in a single TM format), which allows a direct comparison of our multiplexed assay to a non-multiplexed clinical "gold-standard". The TM samples were B·R·A·H·M·S KRYPTOR calibrators provided by Cezanne/Thermo Fisher Scientific. Within the homogeneous FRET immunoassays two different monoclonal primary IgG-antibodies were used against each TM, of which one was labeled with the FRET donor (donor AB), whereas the other one was labeled with the FRET acceptor (acceptor AB). Tb-labeled donor ABs and dye-labeled acceptor ABs were provided by Cezanne/Thermo Fisher Scientific. Details about antibodies and labeling ratios can be found in the Supporting Information.

Table 1. Photophyscial Properties of the Donor (Lumi4-Tb) and the Acceptors As Provided by the Suppliers if Not Indicated Differently[a]

fluorophore	λ_{max} (nm)	ε_{max} (M^{-1} cm^{-1})	τ	Φ
Lumi4-Tb	340	26 000	1.78 ms[b]	0.52[c]
dye1 (OG488)	498	85 000	4.1 ns	0.90
dye2 (AF555)	553	155 000	0.3 ns	0.09
dye3 (AF568)	579	88 000	3.6 ns	0.63
dye4 (Cy5)	649	250 000	1.0 ns	0.27
dye5 (AF700)	696	205 000	1.0 ns	0.08

[a] λ_{max}, absorption wavelength maximum; ε_{max}, molar absorptivity at λ_{max}; τ, luminescence decay time; Φ, luminescence quantum yield. [b] Amplitude-averaged luminescence lifetime of the Lumi4-Tb-labeled antibodies measured in buffer containing 1/3 of serum. The PL lifetime of Lumi4-Tb in aqueous solutions is ca. 2.3 ms. [c] Tb-centered quantum yield (which needs to be used for FRET because the Tb ion is the donor) calculated by Φ = 1.78 ms/3.45 ms (with 3.45 ms measured in D_2O approximated as radiative lifetime). The overall Lumi4-Tb (ligand and Tb ion) Φ is 0.46. Lumi4-Tb in aqueous solution has $\Phi \approx 0.6$ and a Tb-centered Φ = 0.67.

Crosstalk Calibration and Multiplexed Assays. For each single-TM assay, 50 μL of a donor AB mixture (0.08 μg/mL of Tb-labeled NSE, CEA, and Cyfra21.1 ABs, 0.10 μg/mL of Tb-labeled SCC ABs, and 0.14 μg/mL of Tb-labeled CA15.3 ABs in 100 mM Tris buffer containing 0.1% BSA) was added to 50 μL of an acceptor AB mixture (4.0 μg/mL of dye-labeled NSE, CEA, and Cyfra21.1 ABs, 5.0 μg/mL of dye-labeled SCC ABs, and 7.1 μg/mL of dye-labeled CA15.3 ABs in 100 mM Tris buffer containing 0.1% BSA). To this 100 μL donor–acceptor AB mixture was added 50 μL of serum containing the single TMs (from 0.5× to 10× the highest normal concentration value). The highest normal concentrations (1×) for each marker are 12.5 ng/mL for NSE, 3 ng/mL for SCC, 5 ng/mL for CEA, 3 ng/mL for Cyfra21-1 and 30 U/mL for CA15.3 (cf. last line of Table 3). The obtained calibration curves (Figure 2 right for CEA and Supporting Figures 3–6 for NSE, SCC, Cyfra21-1 and CA15.3, respectively) were used to assign a TM-concentration to the A_1 to A_5 intensity values (eq 1). For the multiplexed assays with simultaneous increase of all marker concentrations (Figure 3) the serum samples contained equal concentrations of each TM, which increased from 0.5× to 10× the highest normal value (1×). For the multiplexed assays with "worst case scenario" for spectral crosstalk (Figure 4) the serum samples contained different concentrations of each TM. The NSE concentration was constant at 10× of its highest normal value, the concentrations of SCC and Cyfra21-1 increased from 0.5× to 10×, the CEA concentration decreased from 10× to 0.5×, and the concentration of CA15.3 was constant at 0.5× of its highest normal value. All assays were incubated

dx.doi.org/10.1021/ja310317n | J. Am. Chem. Soc. 2013, 135, 1102–1109

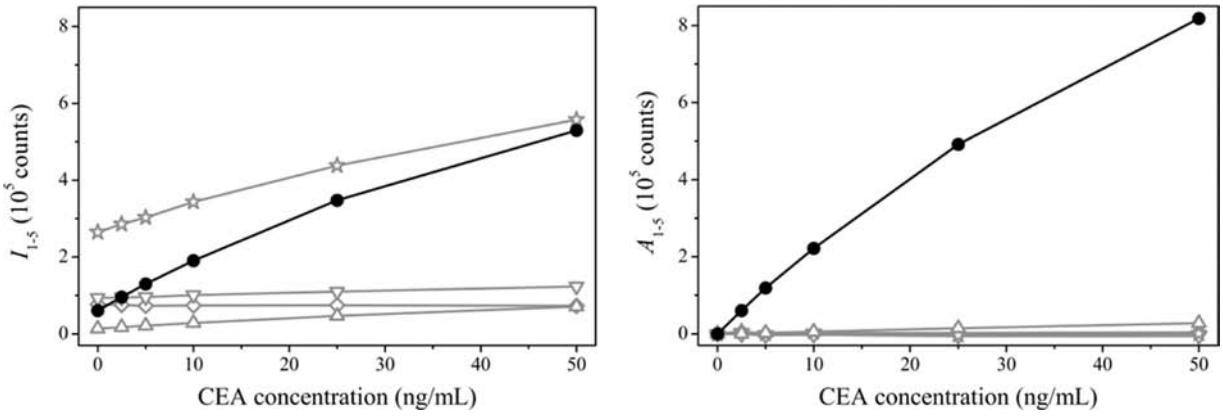

Figure 2. Single tumor marker assay results for CEA concentrations of 0−50 ng/mL before (left) and after spectral crosstalk correction (right) using eq 1. Tb and dye-labeled antibodies for all five tumor markers are present in the assay. As only CEA is added to the samples, only the CEA-specific FRET complex will be formed, and only the Tb donors and the dye3 acceptor (specific for CEA) will show long-lived luminescence, which can be measured within the time-gated detection window. The black curves (●) represent the time-gated dye3 channel intensities. The gray curves (open symbols) represent the time-gated signals within the other dye channels (□, dye1; ▽, dye2; ☆, dye4; △, dye5), which are specific for the other four tumor markers. Before correction there is significant spectral crosstalk of Tb and dye3 emission to other dye channels (intensities I_1−I_5 in eq 1). After correction only the time-gated emission signal of dye3 increases with increasing CEA concentration, and the other dye signals remain at negligibly low signal levels.

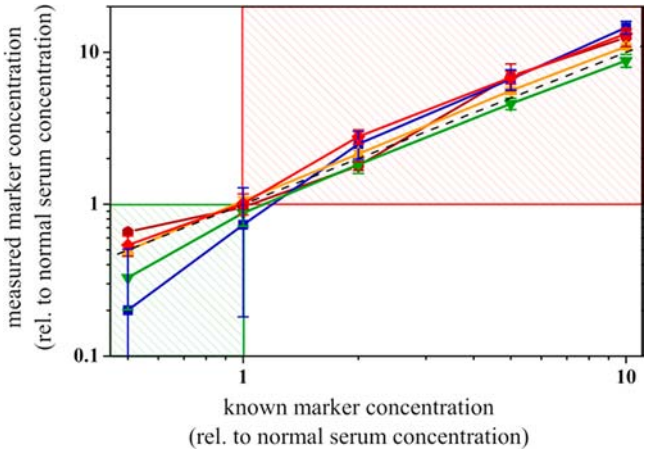

Figure 3. Crosstalk corrected normalized concentrations of the 5-fold multiplexed FRET assay. The green area presents healthy concentrations (0.5−1× highest concentration found in healthy persons; cf. Table 3). The red area presents elevated concentrations (>1× highest concentration found in healthy persons). Due to instantaneous crosstalk correction, the concentrations of samples without tumor markers (concentration zero) are always exactly zero (without deviation) and are therefore not displayed in the graph.

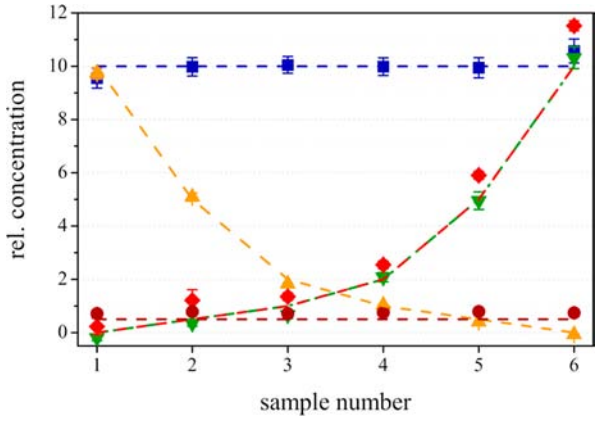

Figure 4. Five-fold multiplexed assay with worst-case spectral crosstalk, where the concentrations of the different tumor markers are held at constant high or low levels or changed from high to low (or low to high) concentrations within six different human serum samples. Symbols represent measured concentrations, and dashed lines indicate known concentrations within the six samples. The different colors indicate the different dyes and tumor markers: blue, dye1 (NSE); green, dye2 (SCC); orange, dye3 (CEA); red, dye4 (Cyfra21-1); brown, dye5 (CA15.3).

for 45 min at 37 °C prior to measurements. Note that the TM concentrations in the 150 μL measuring samples are 3 times lower than in the serum samples (50 μL serum + 100 μL donor−acceptor AB mixture). As the concentration in the serum is the important diagnostic value, all calculated TM concentrations within the assays (e.g., the LODs) are presented as the concentrations in the 50 μL serum samples.

Modified KRYPTOR Immunoreader. Within the modified KRYPTOR system a custom-made dichroic mirror with a sharp transmission cutoff between 500 and 510 nm (Delta, Hørsholm, Denmark) was used to separate the Tb donor emission (first Tb emission line at ca. 495 nm) from the dye acceptor emission bands. As the KRYPTOR offers only two PMT detection channels (one donor and one acceptor emission channel for ratiometric measurements), the five different dye acceptor emissions were measured consecutively by changing the acceptor bandpass filters. For the Tb donor a 494 ± 5 nm bandpass filter (CVI Melles Griot, Albuquerque, NM) was used. The dye acceptor emissions of OG488, AF555, AF568, and AF700 were detected with bandpass filters 521 ± 6, 570 ± 3.5, 608 ± 4, and 708 ± 8 nm (Delta, Hørsholm, Denmark), respectively. The Cy5 acceptor emission was detected with a 659 ± 10 nm bandpass filter (Semrock Inc., Rochester, NY). The filter spectra are displayed in Figure 1. The detection setup of the KRYPTOR immunoreader is shown in Supporting Figure 14. For all assays a 337.1 nm nitrogen laser with 20 Hz repetition rate and ca. 60 μJ pulse energy was used as excitation source. Each well was measured with 100 flashes (5 s per measurement), and the assay volume was always 150 μL. Time-gated luminescence intensities of donor and acceptors were acquired from 50 to 450 μs.

Limits of Detection. "Common" LODs were calculated by using 3 times the standard deviation (SD) of 28 measurements of samples without any markers (but containing all five different Tb−dye AB pairs), thus creating a deviation from the ideal zero-value. As the assay curves for all tumor markers are very close to the ideal 1:1 curve, the

dx.doi.org/10.1021/ja310317n | J. Am. Chem. Soc. 2013, 135, 1102−1109

3×SD values correspond to the LOD. "Realistic" LODs were calculated by using 23 measurements (for each marker) containing 0.5× or 1× the highest normal concentration of one of the markers. This allowed generating a background contribution for each of the five markers within each of the five dye channels. 3×SD of the average background concentration value for each detection channel was used to calculate these LODs. Details about the LOD calculations can be found in Supporting Figures 11−15.

RESULTS AND DISCUSSION

Time-Resolved FRET Immunoassay Format. Homogeneous assays based on FRET from lanthanide-labeled antibodies (Ln-AB) to dye-labeled antibodies (dye-AB) within a "(Ln-AB)−TM−(dye-AB)" immune complex do not require any washing or separation steps. Fast liquid-phase kinetics allow short incubation times, and time-resolved detection permits nearly background-free measurements. Due to their long excited-state lifetimes (up to several milliseconds), lanthanides are ideally suited for time-gated detection approaches, leading to very efficient background suppression in biological applications.[40−44] Apart from supramolecular complexes (such as the Lumi4-Tb complex used in our study), lanthanides have also been used in nanoparticles for time-resolved FRET biosensing. Currently, such approaches provide much higher LODs compared to their supramolecular counterparts and therefore usually cannot access the sub-nanomolar or even sub-picomolar concentration range.[45] In a Tb-based multiplexed immunoassay, the emission spectra of the different dyes can be chosen to fit between or beyond the well-separated emission bands of Tb. Figure 1 shows the spectra of the Tb donor and the five acceptor dyes used within our study. Spectral separation is achieved by using standard optical bandpass filters. However, there is a significant overlap between the different dye emission spectra, leading to spectral crosstalk predominantly from dye emissions of shorter wavelengths into the bandpass filters of longer wavelength dyes. As such crosstalk interference is the main limitation for achieving very low detection limits, we used a precise crosstalk correction, which will be described in detail below. Scheme 1 shows the principle of the homogeneous multiplexed assays. The stock reagent solution contains the matched TM-specific ABs, one conjugated with the common Tb donor and the other conjugated to the TM-specific acceptor dyes. Pulsed UV excitation leads to emission of Tbs and dyes directly after the excitation pulse. However, after a delay of several microseconds, only the Tbs (with millisecond luminescence lifetimes) can be detected, whereas the dye fluorescence signals have already completely decayed (Scheme 1 left). After addition of a serum sample with multiple TMs to the solution, stable TM-specific FRET complexes are formed due to the binding of the two ABs (labeled with Tb and dye, respectively) to their respective TM. Within these specific sandwich complexes, the Tbs can transfer their energy to the respective dyes. As this FRET process depends on the long lifetime of the Tb donor, and Tb and dye are in close proximity, the sensitized dye fluorescence also shows a long decay time (cf. Supporting Figure 2) and can be detected after the microsecond delay in the time-gated detection mode (Scheme 1 right). Thus, the time-gated luminescence intensity of the dyes is directly proportional to the concentration of their respective TM.

Spectral Crosstalk Correction. The spectral crosstalk between the different FRET acceptor dye channels (time-gated emission intensities) is quantified in Table 2. The values in the first column can be compared with the spectrum of dye1 (blue curve from Figure 1). The emission intensity of dye1 in the dye1 channel is normalized to unity. Although the intensity of dye1 continuously decreases beyond its maximum at 530 nm, there is still significant spectral crosstalk contribution to the intensity of the other channels (ca. 14% to dye2 channel, 2.5% to dye3 channel, and 0.4% to dye4 channel). The same principle is applied to all the other dye columns. The last column of Table 2 represents the spectral crosstalk contribution of the Tb donor emission (Figure 1) to the different dye channels. Spectral crosstalk contribution of the dyes to the Tb channel intensity (last row in Table 2) can be neglected due to the much lower intensity compared to the Tb emission at this wavelength.

The relation between the absolute intensities arising from the emission of all different dyes within the different detection channels (I_1−I_5) and the intensities emitted by each single dye (A_1−A_5) can be expressed by eq 1, where **M** is the 5×5 crosstalk correction matrix consisting of the first five columns and rows of Table 2. Matrix **M** can be inverted numerically in order to calculate A_1−A_5 from the measured absolute intensities I_1−I_5 via the right-hand side of eq 1.

Scheme 1. 15-Component Multiplexed FRET Lung Cancer Immunoassay for the Simultaneous Detection of Five Different Tumor Markers[a]

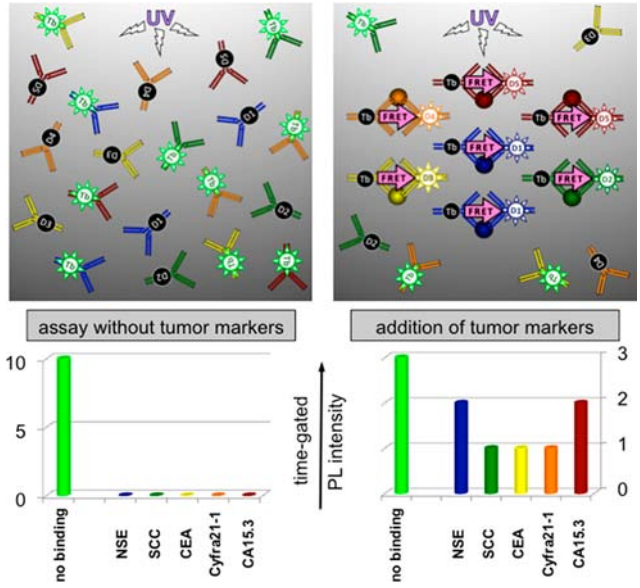

[a]The top images show the different antibody (AB) pairs labeled with terbium complexes (Tbs) and five different organic dyes (D1−D5) before (left) and after (right) addition of the different tumor markers (TMs) (small spheres). ABs of the same color but labeled with Tb or dye are different primary ABs to different epitopes of the respective marker. TM−AB recognition leads to the formation of (Tb-AB)−TM−(dye-AB) sandwich complexes and concomitant efficient FRET from Tbs to the dyes. Star-shaped Tbs or dyes indicate luminescence, whereas the black spheres indicate dark states. The bottom graphs indicate the resulting time-gated luminescence intensities, which are directly proportional to the concentration of each different TM.

dx.doi.org/10.1021/ja310317n | J. Am. Chem. Soc. 2013, 135, 1102−1109

Table 2. Normalized Spectral Crosstalk Intensity Contributions of the Different Dyes and Tb Measured within the Different Optical Bandpass Filter Channels (Time-Gated Emission Intensity)[a]

detection channel	dye1	dye2	dye3	dye4	dye5	Tb
dye1 channel (522 nm)	***1.000 ± 0.017***	***0.000 ± 0.065***	***0.000 ± 0.011***	***0.000 ± 0.001***	***0.005 ± 0.004***	0.094 ± 0.001
dye2 channel (570 nm)	***0.140 ± 0.011***	***1.000 ± 0.022***	***0.076 ± 0.010***	***0.000 ± 0.003***	***0.009 ± 0.007***	0.093 ± 0.001
dye3 channel (607 nm)	***0.025 ± 0.014***	***0.372 ± 0.030***	***1.000 ± 0.008***	***0.002 ± 0.004***	***0.035 ± 0.014***	0.069 ± 0.001
dye4 channel (660 nm)	***0.004 ± 0.019***	***0.234 ± 0.050***	***0.645 ± 0.055***	***1.000 ± 0.004***	***0.057 ± 0.013***	0.361 ± 0.005
dye5 channel (707 nm)	***0.000 ± 0.005***	***0.033 ± 0.017***	***0.091 ± 0.021***	***0.212 ± 0.006***	***1.000 ± 0.004***	0.007 ± 0.0003
Tb channel (495 nm)	0	0	0	0	0	1

[a]The highlighted part is the 5×5 crosstalk correction matrix **M** (cf. eq 1). The values within **M** represent Tb and autofluorescence background corrected values (cf. eq 2). Therefore, the error-included values can be larger than 1 or smaller than 0.

$$\begin{pmatrix} I_1 \\ I_2 \\ I_3 \\ I_4 \\ I_5 \end{pmatrix} = \mathbf{M} \cdot \begin{pmatrix} A_1 \\ A_2 \\ A_3 \\ A_4 \\ A_5 \end{pmatrix} \Rightarrow \begin{pmatrix} A_1 \\ A_2 \\ A_3 \\ A_4 \\ A_5 \end{pmatrix} = \mathbf{M}^{-1} \cdot \begin{pmatrix} I_1 \\ I_2 \\ I_3 \\ I_4 \\ I_5 \end{pmatrix} \quad (1)$$

For accurate results, the I_1−I_5 values must represent only FRET-sensitized acceptor emission. Therefore, any background signal must be subtracted prior to correction. The main time-gated luminescence background signal originates from Tb donor emission, which produces significant crosstalk contribution to the different acceptor dye channels (Table 2, right column). This signal can be determined very accurately by performing a simultaneous measurement of Tb donor emission and dye acceptor emission within the dual detection channel setup of the KRYPTOR immunoreader. This allows a subtraction of the donor channel signal S_{Tb} multiplied by the spectral crosstalk ratio f_{Tb} (Table 2, right column) from the acceptor channel signal S_i ($[S_i - f_{Tb}S_{Tb}]$ in eq 2). Due to time-gating after a microsecond delay, autofluorescence background from the sample is almost negligible. However, in order to achieve even better sensitivity, this background contribution is also taken into account ($[S_i(0) - f_{Tb}S_{Tb}(0)]$ in eq 2), where $S_i(0)$ and $S_{Tb}(0)$ denote the measured signals in the dye and the Tb channels without TMs inside the sample (pure serum). The pure FRET signal I_i (with $i = 1$−5) is then determined by

$$I_i = [S_i - f_{Tb}S_{Tb}] - [S_i(0) - f_{Tb}S_{Tb}(0)] \quad (2)$$

The evaluation of Tb crosstalk contribution to the dye channels in combination with the simultaneous detection of the emission signals of dyes and Tb during the immunoassays allows a very precise subtraction of all background signals of each individual measurement. Therefore, our method is equivalent to the ratiometric measurements (dye signal divided by Tb signal) performed for most commercial single tumor marker assays in order to account for fluctuations in serum samples and excitation light intensity. Luminescence decay time analysis by automatic comparison of measured to expected decay times for each FRET pair and the division of the time-resolved luminescence intensity from 20 μs to 4 ms into 11 intervals (with weighting factors indirectly proportional to the respective uncertainty associated to each interval) further optimized the detection at low signal-to-background levels.

For the concentration calibration of the immunoassays (A_1−A_5 values as a function of the known concentrations of the five different tumor markers) as well as for the practical evaluation of the crosstalk correction assay, calibration curves were measured for each dye. Figure 2 shows the measured intensities obtained from the single CEA tumor marker assay before and after spectral crosstalk correction according to eq 1 (cf. Supporting Information for details concerning all other markers). Different levels of Tb background emission in the different dye channels as well as crosstalk of dye3 (specific for CEA) to other dye channels (most prominently to the dye4 channel) are clearly visible in the signals I_1−I_5. The crosstalk-corrected signals A_1−A_5 demonstrate the high efficiency of our correction algorithm, as only the dye3 signal increases significantly.

5-Fold Multiplexed Lung Cancer Assay. For an overall evaluation of the 5-fold multiplexed assay, tumor marker concentrations were considered with respect to their highest values occurring within physiological serum samples of healthy persons (last row in Table 3, below). The FRET-sensitized time-gated emission intensity of the different dyes was detected and crosstalk-corrected to yield the different values of A_1−A_5 for known sample concentrations ranging from 0.5- to 10-fold the highest concentration of all five markers in healthy persons. The obtained values were used to calculate the measured concentrations (using the single calibration curves such as Figure 2, right, for CEA). These values were then compared to the known concentrations in order to evaluate the multiplexed assay format (Figure 3). The excellent agreement between known and measured concentrations demonstrates the suitability of our crosstalk-corrected FRET technology to measure very low amounts of biomolecules, even in the 5-fold multiplexed format, and to efficiently distinguish between healthy concentrations (green area) and elevated concentrations (red area). Deviations from the ideal linear curve (diagonal dashed line) are in general relatively small over the complete concentration range spanning 2 orders of magnitude. These deviations are generally larger than the error bars shown in the graph because these errors only indicate the accuracy of the spectroscopic measurement and data processing. Any factors influencing the biomolecular binding conditions (which are independent of spectral crosstalk correction) are not included in the errors. It should be mentioned that a sandwich immunoassay is one of the most challenging biosystems for monitoring multiple binding events. Two antibodies and one marker per immunocomplex result in a total of 15 different biomolecules involved in biological recognition within our 5-fold multiplexed FRET assay (cf. Supporting Information for details of "biochemical errors" within the tested lung cancer assay system). Nevertheless, the observed deviations are quite small, and a biochemical optimization of all antibody pairs toward their application in a multiplexed assay would most probably allow an even closer approach to the ideal curve. The investigation of a multiplexed system with direct binding of donor- and acceptor-labeled molecules (e.g., protein−protein

Table 3. Limits of Detection of Commercial Single Assays and Crosstalk-Corrected Multiplexed Assays, and Highest Marker Concentrations in Physiological Human Serum

	NSE in pM (ng/mL)	SCC in pM (ng/mL)	CEA in pM (ng/mL)	Cyfra21-1 in pM (ng/mL)	CA15.3 in U/mL[d]
LOD commercial single assay[a]	10.0 (0.8)	2.1 (0.1)	1.1 (0.2)	5.3 (0.16)	0.3
"common" LOD multiplexing (no other TMs present)	75.0 (6.0)	6.7 (0.32)	0.5 (0.09)	14.3 (0.43)	0.03
"realistic" LOD multiplexing (other TMs present)	150 (12)	18.1 (0.87)	1.1 (0.19)	24.7 (0.74)	0.16
highest normal concentration[b]	156 (12.5)	62.5 (3.0)	27.8 (5.0)	100 (3.0)	30[c]

[a]Provided by BRAHMS/Thermo Fisher Scientific for optimized standard clinical KRYPTOR system. [b]Highest values occurring in healthy persons.[37,38] [c]Due to the very high sensitivity of the CA15.3 assay, the 1× highest normal concentration in our assays was 30-fold lower (1 U/mL instead of 30 U/mL). See Supporting Information for details. [d]U/mL for CA15.3 cannot be transferred into molar units.

interactions in cellular imaging) would already reduce the number of binding-active species by 1/3, and thus lead to a significant reduction of cross-reactivity problems and a concomitant higher detection accuracy for such applications.

Multiplexed Lung Cancer Assay with Worst-Case Spectral Crosstalk. In order to support our argument that the main errors or uncertainties in the multiplexed assay arise from effects of biochemical binding and not from unexpected deviations in spectral crosstalk, we performed a "worst-case scenario" assay for spectral crosstalk. This test comprises NSE (dye1), with significant crosstalk contribution to other dye channels, at highest concentration. At the same time the markers for the next dye channels—SCC (dye2), CEA (dye3), and Cyfra21-1 (dye4)—were varied from highest to zero concentrations and vice versa. Finally, CA15.3 (dye5), with significant crosstalk from other dyes in the corresponding dye5 channel, was kept constant at the lowest concentration level within the multiplexed assay. Figure 4 demonstrates the robustness of our optically multiplexed method, as the measured concentrations are in very good agreement with the known concentrations within the six samples containing the different tumor marker mixtures. The only significant deviation can be found for the signal of dye4, which is consistently higher than expected for all concentrations and can be attributed to the cross-sensitivity problems mentioned above. On the other hand, the expected concentrations are reproduced almost ideally for dye3, although the dye3 channel is affected by a large amount of spectral crosstalk from other dyes. This clearly shows the reliability of our optical detection and crosstalk correction method if cross-reactivity problems are negligible, which is the case for the CEA marker−antibody system.

Another interesting aspect concerning multiplexed analysis within the different samples shown in Figure 4 is the difference in marker concentrations, which allows a distinction between SCLC and NSCLC. Using an algorithm by Molina et al. to suggest the histological diagnosis of lung cancer,[35] samples 1 and 2 ([SCC] < 2 ng/mL and [NSE] > 45 ng/mL) can be clearly identified as SCLC (stage I−IV or extensive disease), whereas the other samples are NSCLC ([SCC] > 2 ng/mL). In the case where NSE would have a low concentration (<35 ng/mL; not the case here but would lead to even better results for the crosstalk correction), all samples would suggest NSCLC (stage I−IV or extensive disease), for which the sensitive distinction among the Cyfra21-1, CEA, and CA15.3 concentrations within our assay is of high importance. Our results clearly demonstrate that this suggested histological diagnosis can be successfully reproduced with our 5-fold FRET technology.

Detection Limits. Regarding the sensitivity of our multiplexed biosensor, we estimated the LODs by two different approaches. The "common" LOD was determined as the zero standard value plus three standard deviations. The different LODs are far below (2-fold for NSE) the highest concentrations in healthy persons (Table 3). Taking into account the multiplexed format of our assay, it cannot be assumed that all tumor markers approach the zero concentration simultaneously. Therefore, we also calculated a "realistic" LOD, determined as the zero standard value plus three standard deviations of the background contribution from each of the five markers within each of the five dye channels. They are still significantly below (equal to for NSE) the highest healthy concentration values and only moderately larger than the "common" LODs. Comparing the LODs to those of fully optimized commercial immunoassays (first row in Table 3) provides interesting information. First, our CA15.3 detection is much more sensitive (especially for the "common" LOD), because there is almost no Tb background at the dye5 wavelength. Second, CEA shows a better "common" and equal "realistic" LOD, demonstrating that a very reproducible antibody−antigen binding pair (*vide supra*) within our multiplexed format can already provide sensitivities comparable to those of an optimized commercial single-marker assay. Third, the LODs for NSE are much higher in our assays, which shows that antibody−antigen binding problems can cause significant loss in sensitivity but also that substantial improvement can be expected when optimized antibodies are used. It is important to mention that the LODs state the minimum reliably detectable concentrations and do not necessarily give information on the accuracy of the measurement at higher concentrations. This accuracy strongly depends on the reproducibility of the measurement, which is mainly influenced by the binding affinity between antibodies and marker. Stability of antibody and marker solutions and exact control of incubation conditions are therefore mandatory to get precise results. Regarding the difference between the LODs achieved with our modified research setup and the optimized and fully automated commercial system, we expect another significant decrease of the LODs for our multiplexed assays after industrial optimization and automation. Nevertheless, our results clearly demonstrate that, already without further optimization, our multiplexed FRET technology provides very high sensitivity, as demonstrated by the precise detection within clinically relevant concentration ranges.

■ CONCLUSION

Multiple biomarker sensing and simultaneous monitoring of several biomolecular interactions for understanding their interplay within complex biological systems are of large interest for many fundamental questions in the life sciences. Multi-

plexed optical detection with very high sensitivity in a biological environment (e.g., serum or cell culture) is a powerful tool for realizing such sophisticated biosensing experiments. Using simultaneous time-resolved six-color FRET from one Tb complex donor to five different organic dye acceptors, we demonstrated that monitoring of multiple molecular binding events at very low concentrations is feasible even for challenging biosystems. Low picomolar detection limits for five different lung cancer tumor markers were achieved in a very challenging immunoassay, which combined 15 different biomolecules (10 antibodies interacting with 5 tumor markers). The unique combination of high-sensitivity fluorescence detection with straightforward spectral crosstalk correction allowed an efficient distinction between healthy and elevated biomarker levels as well as a prediction of the type of lung cancer (SCLC or NSCLS) from a single 50 μL human serum sample. We expect our method to provide significant benefits for real-time investigations of simultaneous biomolecular interactions and ultrasensitive detection of multiple biomarkers for early disease diagnostics.

■ ASSOCIATED CONTENT

Supporting Information

(1) Details concerning antibodies and labeling ratios; (2) overlap integrals $J(\lambda)$ and Förster distances R_0 of the used donor−acceptor pairs; (3) FRET-quenched donor and FRET-sensitized acceptor luminescence decay curves; (4) measured intensities obtained from the NSE, SCC, Cyfra21-1, and CA15.3 single-TM assays before and after spectral crosstalk correction; (5) sensitive detection of CA15.3 from the human serum component in the single-TM assays for NSE, SCC, CEA, and Cyfra21-1. (6) investigation of biochemical errors; (7) single immunoassay control experiments using Cyfra21-1 and CA15.3 antibodies with either Cyfra21-1 or CA15.3 TM in order to validate cross sensitivity of the antibody−TM pairs; (8) single immunoassay control experiments with NSE antibodies and NSE TM at different concentrations and incubation times in order to validate if the weak FRET signals for NSE result from unfavorable binding conditions for NSE; (9) calculation of the "common" and the "realistic" LODs of all TMs within the 5-fold multiplexed assays; (10) detection setup of the KRYPTOR immunoreader for the time-resolved FRET measurements; (11) crosstalk and background correction and treatment of experimental uncertainties. This material is available free of charge via the Internet at http://pubs.acs.org.

■ AUTHOR INFORMATION

Corresponding Author

niko.hildebrandt@u-psud.fr

Notes

The authors declare no competing financial interest.

■ ACKNOWLEDGMENTS

The authors thank the European Commission (FP6 project POC4life and FP7 project NANOGNOSTICS) for financial support.

■ REFERENCES

(1) Söderberg, O.; Gullberg, M.; Jarvius, M.; Ridderstrale, K.; Leuchowius, K. J.; Jarvius, J.; Wester, K.; Hydbring, P.; Bahram, F.; Larsson, L. G.; Landegren, U. *Nat. Methods* **2006**, *3*, 995−1000.

(2) Hampel, S.; Chung, P.; McKellar, C. E.; Hall, D.; Looger, L. L.; Simpson, J. H. *Nat. Methods* **2011**, *8*, 253−U102.

(3) Breton, B.; Sauvageau, E.; Zhou, J.; Bonin, H.; LeGouill, C.; Bouvier, M. *Biophys. J.* **2010**, *99*, 4037−4046.

(4) Mori, M.; Imai, Y.; Itsuki, K.; Inoue, R. *Biochemistry* **2011**, *50*, 4685−4696.

(5) Essaka, D. C.; Prendergast, J.; Keithley, R. B.; Palcic, M. M.; Hindsgaul, O.; Schnaar, R. L.; Dovichi, N. J. *Anal. Chem.* **2012**, *84*, 2799−2804.

(6) Förster, T. *Discuss. Faraday Soc.* **1959**, *27*, 7−17.

(7) Van der Meer, B. W.; Coker, G.; Chen, S. S. *Resonance Energy Transfer: Theory and Data*; Wiley-VCH: Weinheim, 1994.

(8) Lakowicz, J. R. *Principles of Fluorescence Spectroscopy*, 3rd ed.; Springer: Berlin, 2006.

(9) Clegg, R. M. Förster resonance energy transfer—FRET what is it, why do it, and how it's done. in *Laboratory Techniques in Biochemistry and Molecular Biology*; Gadella, T. W. J., Ed.; Academic Press: Burlington, 2009; Vol. 33, pp 1−57.

(10) Szöllosi, J.; Damjanovich, S.; Mátyus, L. *Cytometry* **1998**, *34*, 159−179.

(11) Stryer, L. *Annu. Rev. Biochem.* **1978**, *47*, 819−846.

(12) Sahoo, H. *J. Photochem. Photobiol. C—Photochem. Rev.* **2011**, *12*, 20−30.

(13) Selvin, P. R. *Nat. Struct. Biol.* **2000**, *7*, 730−734.

(14) Jares-Erijman, E. A.; Jovin, T. M. *Nat. Biotechnol.* **2003**, *21*, 1387−1395.

(15) Pietraszewska-Bogiel, A.; Gadella, T. W. J. *J. Microsc.* **2011**, *241*, 111−118.

(16) Grecco, H. E.; Verveer, P. J. *ChemPhysChem* **2011**, *12*, 484−490.

(17) Sun, Y.; Wallrabe, H.; Seo, S.; Periasamy, A. *ChemPhysChem* **2011**, *12*, 462−474.

(18) Shcherbakova, D. M.; Subach, O. M.; Verkhusha, V. V. *Angew. Chem., Int. Ed.* **2012**, *51*, 2−17.

(19) Stein, I. H.; Steinhauer, C.; Tinnefeld, P. *J. Am. Chem. Soc.* **2011**, *133*, 4193−4195.

(20) Wang, Z. G.; Elbaz, J.; Willner, I. *Nano Lett.* **2011**, *11*, 304−309.

(21) Burns, J. R.; Preus, S.; Singleton, D. G.; Stulz, E. *Chem. Commun.* **2012**, *48*, 11088−11090.

(22) Hötzer, B.; Medintz, I. L.; Hildebrandt, N. *Small* **2012**, *8*, 2297−2326.

(23) Sapsford, K. E.; Berti, L.; Medintz, I. L. *Angew. Chem., Int. Ed.* **2006**, *45*, 4562−4589.

(24) Resch-Genger, U.; Grabolle, M.; Cavaliere-Jaricot, S.; Nitschke, R.; Nann, T. *Nat. Methods* **2008**, *5*, 763−775.

(25) Geißler, D.; Charbonnière, L. J.; Ziessel, R. F.; Butlin, N. G.; Löhmannsröben, H.-G.; Hildebrandt, N. *Angew. Chem., Int. Ed.* **2010**, *49*, 1396−1401.

(26) Hildebrandt, N. *ACS Nano* **2011**, *5*, 5286−5290.

(27) Haugland, R. P. *The Molecular Probes Handbook—A Guide to Fluorescent Probes and Labeling Technologies*, 11 ed.; Life Technologies Corp.: Carlsbad, CA, 2010.

(28) Hermanson, G. T. *Bioconjugate techniques*; Academic Press: San Diego, 1996.

(29) Kokko, T.; Liljenbäck, T.; Peltola, M. T.; Kokko, L.; Soukka, T. *Anal. Chem.* **2008**, *80*, 9763−9768.

(30) Kokko, T.; Kokko, L.; Soukka, T. *J. Fluor.* **2009**, *19*, 159−164.

(31) Kupcho, K. R.; Stafslien, D. K.; DeRosier, T.; Hallis, T. M.; Ozers, M S.; Vogel, K. W. *J. Am. Chem. Soc.* **2007**, *129*, 13372−13373.

(32) Kim, S. H.; Gunther, J. R.; Katzenellenbogen, J. A. *J. Am. Chem. Soc.* **2010**, *132*, 4685−4692.

(33) Boyle, P.; Levin, B. World Cancer Report 2008. International Agency for Research on Cancer: Lyon, 2008

(34) American Cancer Society. *Cancer Facts & Figures 2008*; American Cancer Society: Atlanta, 2008.

(35) Travis, W. D.; Travis, L. B.; Devesa, S. S. *Cancer* **1995**, *75*, 191−202.

(36) Molina, R.; Filella, X.; Augé, J. M. *Eur. Oncol. Dis.* **2006**, *1*, 106−109.

(37) Xu, J.; Corneillie, T. M.; Moore, E. G.; Law, G.-L.; Butlin, N. G.; Raymond, K. N. *J. Am. Chem. Soc.* **2011**, *133*, 19900−19910.

(38) Molina, R.; Filella, X.; Auge, J. M.; Fuentes, R.; Bover, I.; Rifa, J.; Moreno, V.; Canals, E.; Vinolas, N.; Marquez, A.; Barreiro, E.; Borras, J.; Viladiuc, P. *Tumor Biol.* **2003**, *24*, 209−218.
(39) Molina, R.; Auge, J. M.; Escudero, J. M.; Marrades, R.; Vinolas, N.; Carcereny, E.; Ramirez, J.; Filella, X. *Tumor Biol.* **2008**, *29*, 371−380.
(40) Selvin, P. R. *Annu. Rev. Biophys. Biomol. Struct.* **2002**, *31*, 275−302.
(41) Charbonnière, L. J.; Hildebrandt, N. *Eur. J. Inorg. Chem.* **2008**, *2008*, 3241−3251.
(42) Mathis, G. *Clin. Chem.* **1993**, *39*, 1953−1959.
(43) Mathis, G. *Clin. Chem.* **1995**, *41*, 1391−1397.
(44) Mathis, G. *J. Biomol. Screen.* **1999**, *4*, 309−313.
(45) Lui, Y.; Zhou, S.; Tu, D.; Chen, Z.; Huang, M.; Zhu, H.; Ma, E.; Chen, X. *J. Am. Chem. Soc.* **2012**, *134*, 15083−15090.